International Journal of Engineering Trends and Technology
ISSN: 2231–5381 / https://doi.org/10.14445/22315381/IJETT-V74I1P113

Volume 74 Issue 1, 160-173, January 2026

Original Article

Lung Cancer Classification Using Adaptive Correlation Enhanced Active Contour Model and DenseEnsembleNet

Raghapriya.N[1], Aswini.N[2], Savitha.G[3], Beschi.I.S[4]

[1,2,3]*Department of Computer Science and Applications, SRM Institute of Science and Technology, Faculty of Science and Humanities, Ramapuram, Chennai, Tamil Nadu, India.*
[4]*Department of Computer Science and Engineering, Sathyabama Institute of Science and Technology, Jeppiaar Nagar, Chennai, Tamil Nadu, India.*

[1]*Corresponding Author : raghapriyakamal@gmail.com*

Received: 04 July 2025 Revised: 19 December 2025 Accepted: 26 December 2025 Published: 14 January 2026

Abstract *- This study presents a novel approach to lung cancer classification combining deep learning, feature extraction, and image processing. It enhances lung cancer images using advanced denoising techniques, Non-Local Means (NLM), Wavelet, and augments the dataset with Generative Adversarial Networks (GANs) to improve model generalization. The Region of Interest (ROI) is identified with an Adaptive Correlation-Enhanced Active Contour Model (ACE-ACM), and feature extraction using pre-trained CNNs like VGGNet and ResNet. To identify key features of the hybrid optimization algorithm, Sparrow Customized Sea Lion Optimization (SLO) and Sparrow Search Algorithm (SSA). The classification utilizes DenseEnsembleNet, a combination of Optimized DenseNet and CNN, achieving a remarkable accuracy of 98.79%. By using a Python-based platform, the framework provides an innovative solution for accurate lung cancer diagnosis and efficient treatment planning. Provides an innovative solution for accurate lung cancer diagnosis and efficient treatment planning.*

Keywords *- Adaptive Correlation Enhanced Active Contour Model, Lung cancer, DenseEnsembleNet, Denoising techniques, Generative Adversarial Networks, Region of Interest.*

1. Introduction

One of the most serious and dangerous illnesses in the world is lung cancer. The only way to treat lung cancer is to find it in the early stages. Several methods may be used to diagnose lung cancer, such as MRI, isotope, X-ray, and Computer Tomography (CT) [1, 2]. PET, CT, and X-ray chest radiography are the three popular imaging techniques; they are routinely used to identify various lung conditions. CT scans are used by doctors and radiologists to identify and diagnose diseases, describe the patterns and severity of illnesses, the morphologic extents of diseases, and gauge the clinical progression of diseases and how they react to medicines. As CT technology has evolved, the high-resolution CT test has emerged as the imaging method of choice for the recognition and detection of lung disorders [3-5]. The task of visually reading or assessing a large number of CT image slices is still difficult despite High-Resolution CT suggesting images of the lung with a continually growing anatomic solution. In contrast to the categorization of benign and malignant [6-8], the classification of the three forms of lung cancer using medical pictures is more apt to represent an incredibly fine image identification challenge due to distinct feature variations and potential malignant characteristics that must be taken into account. The affected region occupies a small percentage of the whole image, rendering the fine-grained characteristics that must be retrieved from images vulnerable to feature noise [9, 10]. The great majority of techniques now being used that are based on different DL models have shown a particular restriction in fine-grained settings. For the purpose of identifying and categorizing pulmonary diseases, the channel attention mechanism has been employed [11, 12]. The discussion of various attention tactics offers many viewpoints on the origins of noise identification. There are several efforts underway to produce computer-assisted methods for diagnosis and detection that will raise the standard of diagnosis for the categorization of lung cancer [13-15]. Computer-aided systems were created as a result of the need for trustworthy and impartial analyses. To extract characteristics for categorization and severity determination is the goal of this effort. This research introduces an innovative approach to accurately classify lung cancer, a critical task for effective treatment planning. By combining advanced image processing techniques such as denoising and segmentation with deep learning models like VGGNet and ResNet, intricate features are extracted from lung tumor images. A novel hybrid optimization algorithm further refines feature selection, reducing dimensionality and enhancing focus on crucial aspects. The proposed DenseEnsembleNet, a fusion of

optimized DenseNet and CNN, empowers the model to recognize complex patterns. Experimental results on benchmark datasets demonstrate the method's superiority over traditional approaches, offering promising potential to assist healthcare professionals in early-stage lung cancer diagnosis and treatment decision-making. “The main contribution of the paper is as follows”,

To effectively extract the lung tumor region, the Adaptive Correlation Enhanced Active Contour Model (ACE-ACM) is used in the medical images using a segmentation algorithm. In this model, the cross-correlation-based entropy is calculated to improve the performance of the ACM model. To optimize the feature space and reduce dimensionality, we utilize an advanced feature selection algorithm called Sparrow Customized Sealion Optimization (ScLnO), which can include the advantages of both the Sea Lion Optimization (SLO) and Sparrow Search Algorithm (SSA). In this phase, Detection and tracking of prey by scroungers is improved using the SLO algorithm. The producer-scrounger interaction phase is also improved using the vocalization behavior of the SLO. To fine-tune the hyperparameters of the DenseNet model, the ScLnO algorithm is utilized. The optimized DenseNet model is used along with the CNN for the classification of lung cancer disease. The ScLnO algorithm is used to fine-tune the DenseNet model's hyperparameters, such as the number of layers, batch size, and learning rate.

To improve the classification process, the Optimized DenseNet and the CNN models are used. The outputs of these two models are concatenated and gives the final classified lung cancer detection output. The document is constructed in the manner described below. Section 2 includes recent publications on lung cancer detection, Sections 3 provide experimental details, a description of the suggested approach, Section 4 provides a comparison of the outcomes, and Section 5 gives the detailed conclusion.

2. Literature Review

This section discusses recent research publications on lung cancer detection.

In 2022, Kasinathanand Jayakumar [16] have suggested a cloud-based system for the stage-based identification of lung tumors using deep learning. In addition to offering a way for classifying pulmonary illness phases, the study also offers a deep neural network and a cloud-based data collection system for recognizing and validating distinct lung cancer growth stages. The cloud-based Lung Cancer Detector and Stage Classifier, a hybrid PET/CT imaging technology offered by the suggested approach, is used to analyze lung tumors. A multilayer CNN for differentiating between lung cancer kinds has been created and tested using industry-accepted benchmark images. First, the suggested Cloud-LTDSC was used to create the active contour system for lung cancer segmentation. In 2021, Sujitha and Seenivasagam [17] used machine learning and a big data healthcare platform for stage classification of lung cancer. The architecture for the most successful categorization of photos and lung cancer stages was designed in that work using Apache Spark and a streamlining of machine learning techniques. The experiments use the threshold technique (T-BMSVM) to categorize tumors into benign and malignant tumors and identify the degree of cancer, respectively. They incorporate binary classification, multiclass categorization, and multiclass grouping.

In 2020, Asuntha and Srinivasan [18] introduced a deep learning model for the categorization and detection of lung cancer. The scientists found the cancerous lung nodules using cutting-edge Deep learning algorithms. The best feature extraction techniques, such as the Scale Invariant Feature Transform, Histogram of Oriented Gradients (HoG), Zernike Moment, and Local Binary Pattern, are employed in that study. The Fuzzy Particle Swarm Optimization (FPSO) approach is used to choose the ideal feature following the extraction of textural, geometric, volumetric, and intensity data. The classification of these traits is subsequently done using deep learning. Using a groundbreaking FPSOCNN, the computational difficulty of CNNs is reduced.

In 2021, Ibrahim et al. [19] recognized chest conditions, including COVID-19, pneumonia, and lung cancer, and suggested that a multi-classification system based on deep learning may be utilized. A multiple classification deep learning system for the diagnosis of COVID-19, pneumonia, and lung cancer was recommended in that study to be developed using a combination of chest x-ray and CT images. The combo was chosen because a chest X-ray was less beneficial in the early stages of the disease, whereas a chest CT scan was beneficial even before symptoms appeared and could precisely detect the aberrant characteristics that were visible in photos. Utilizing these two separate photo types will also increase the dataset and increase classification accuracy. There is currently no deep learning model that can distinguish between these illnesses.

In 2021, Kumar and Bakariya [20] utilized deep learning to categorize malignant lung cancer. The author of that research recommends GoogLeNet and AlexNet as deep neural networks. A pretrained CNN was used in experiments on LIDC processing datasets. That work describes an automated technique for identifying lung nodules in areas of interest (ROI). A median filter, a Gaussian filter, a Gabor filter, and a watershed algorithm were added to the DICOM picture size 512 512 to partition the lung sections. (Fully linked) Layers were used by AlexNet, and Pooling Layers were used by GoogleNet.

In 2021, Nanglia et. al. [21] suggested a hybrid approach that uses SVM and neural networks to classify lung cancer. The focus of the current study was on the factual information

on the potential application of a hybrid Feed-Forward Back Propagation Neural Network for lung cancer diagnosis. Support Vector Machine (SVM) is used in this situation to develop a hybrid approach that further aids in lowering the computational complexity of the categorization. In light of the previously stated, a three-block system is proposed for categorization, with the first block handling dataset preliminary processing, the following block collecting characteristics using the SURF method, the third block optimizing using an algorithm based on genetics, and the last block executing classification using FFBPNN.

In 2021, Marentakis et. al. [22] used radiomics and deep learning algorithms to determine that lung cancer histology can be determined from CT scans. By using various feature extraction and classification algorithms on pretreatment CT images, this study seeks to evaluate the possibility of NSCLC histological categorization into AC and SCC. The used picture dataset (102 patients) came from the TCIA, which was a collection of publicly accessible cancer imaging archives. The suggested method was founded on pretreatment CT imaging, which offers knowledge about the tumor's geographic heterogeneity as well as its overall picture features. As part of clinical practice prior to therapy, CT imaging does not add any further complication or delay.

In 2022, Shafi et. al. [23] used a deep learning-based support vector network, an efficient method for detecting lung cancer from a CT scan. The SVM used in that work, which was deep learning capable, was proposed as a cancer detection model. The suggested Computer-Aided Design (CAD) model is used to identify the physical and pathological changes in the tissue layers of the cross-section of lung cancer tumors. When lung cancer was first discovered, the model was initially taught to detect it by evaluating and analyzing the preset profile traits in CT scans acquired from patients and control patients. Using CT pictures of individuals and control subjects who had not participated in the training phase, the model was then evaluated and verified.

In 2023, Pandit et. al. [24] recommended a lung cancer categorization deep learning neural network. The suggested technique combines multispacer images in the pooling layer of a CNN, utilizing the Adam Algorithm for optimization to increase overall accuracy and diagnose lung cancer. Prior to down-sampling via max pooling, the CT images underwent pre-processing by being fed into a convolution filter. An autoencoder model based on a CNN was then used to extract features, and multispacer image reconstruction was employed to decrease error during image reconstruction, improving prediction accuracy for lung nodules. Finally, the SoftMax classifier was used to categorize the CT images using the reconstructed pictures as input.

In 2020, Bicakci et. al. [25] suggested the molecular imaging-based sub-classification of lung cancer. Adenocarcinoma (ADC) and Squamous Cell Carcinoma (SqCC), two subtypes of NSCLC, were distinguished in that study using deep learning-based classification algorithms, which were thoroughly studied. The study included PET scans and tumor-containing slices from 94 individuals (88 males), of which 38 had ADC, and the remaining had SqCC. To determine how peritumoral regions in PET scans affect the subtype categorization of tumors, three trials were conducted. Each model was optimized using a variety of optimizers and regularization techniques.

2.1. Problem Statement

The research on lung cancer diagnosis is crucial for better outcomes. Current techniques achieve high levels of accuracy and reliability, leading to incorrect diagnoses and delayed actions. Early detection of lung cancer is essential for better outcomes. New image processing methods and feature extraction strategies are developed to improve medical imaging data quality, particularly CT scans and PET images. The proper categorization of lung cancer stages and subtypes is challenging, necessitating the creation of strong models that distinguish between complex disease presentations. Initiatives reduce computational complexity while maintaining diagnostic efficacy. Integrating data from various medical imaging modalities, such as chest X-rays and CT scans, enhances diagnosis accuracy. Cloud-based solutions and big data frameworks are being researched to handle the growing amount of medical imaging data. Machine learning and deep learning methods are essential for recognizing multifaceted data designs and drawing insightful conclusions. The ultimate goal is to develop diagnostic representations that integrate seamlessly into clinical practice, providing medical practitioners with precise and timely information for informed decision-making. This article aims to enhance lung cancer diagnosis and patient care by addressing gaps in the literature, developing a comprehensive model for distinguishing between COVID-19, pneumonia, and lung cancer, and exploring advanced techniques such as histology classification.

3. Proposed Methodology

Lung cancer classification is crucial for medical diagnostics and treatment planning. Accurate categorization methods are essential for predicting incidence and severity. This section demonstrates accurate classification and prediction using DL and Image Processing technologies. .

Preprocessing images using wavelet and NLM denoising improves visual quality. GANs are used for data augmentation and modified Active Contour Models segment pictures for easier identification of the region of interest. Deep learning classification techniques are applied. A block diagram is provided for the suggested Lung Cancer detection methodology. The block design of the proposed lung cancer detection system is shown in Figure 1.

3.1. Preprocessing

Lung cancer images undergo preprocessing to enhance picture quality and reduce noise. Advanced denoising techniques like NLM and wavelet denoising are used to preserve image details and improve analysis accuracy.

The optimal performance criteria include a search window size of 21 x 21 pixels, patch dimensions of 7 by 7 pixels, adaptive thresholding, and a threshold value of 0.1. These techniques effectively remove high-frequency noise from medical photos.

Using NLM and wavelets, we can use multi-resolution analysis, which decomposes an image into different frequency components. In the high-frequency scale, noise tends to be concentrated, while important features of images are in the low frequency and provide high spatial localization. A wavelet can identify where specific frequency components are located in the image.

This is important for preserving the edges and fine details of lung nodules while suppressing noise. Wavelets can adapt to different types of noise and image characteristics by adjusting parameters such as the wavelet type, thresholding method (soft threshold and hard threshold), and decomposition level. The medical image denoising method based on the wavelet transform is widely used. Traditional denoising methods can remove image noise, but they still ignore the details of image features, and it is difficult to capture the complete contour information.

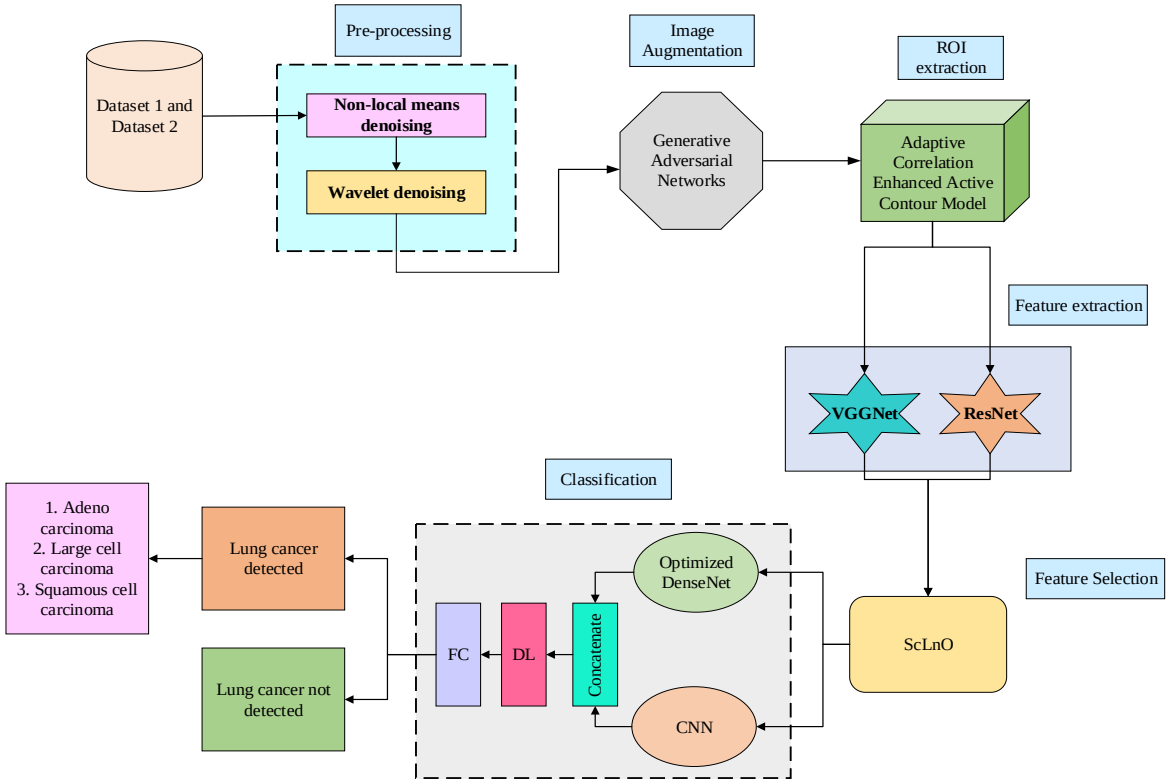

Fig. 1 Block design of the proposed lung cancer detection system

So, the denoised results may not be suitable for some applications that need high accuracy, such as in medical image processing, remote sensing, and so on. A filter named Non-Local Mean (NLM) filter was constructed based on block similarity and global patch similarity, which significantly improved the effect of image denoising. The major importance of using NLM lies in finding similar patches (small regions) throughout the image and averaging pixel values from those similar patches. This helps remove noise without blurring important features. Principal Component Analysis (PCA) can blur images and remove important features. It is clear from the state-of-the-art that PCA can be explored further for image denoising, especially for low-resolution or high noise level images. N2N requires independent noisy images of the same scene, which can be difficult to acquire. After a thorough analysis and benchmarking, it is evident that the existing method of denoising techniques falls short in maintaining a balance between noise reduction and preserving crucial information from images. The Proposed model shows the use of NLM and wavelet methods to reduce noise with high accuracy, and shows that these methods are the best denoising methods among other methods. Soft and Hard thresholding approaches for denoising images using wavelets. Improved wavelet thresholding assisted in the noise reduction of the image. The software thresholding parameter provides the details of the coefficients that contain high-frequency

disturbances as well as certain signal details. The process of soft-thresholding is applied to denoise. Hardware thresholding parameter, applying threshold, the image is transformed using the wavelet transform to obtain a denoised set of wavelet coefficients. Specific numbers to adjust the wavelet hard threshold for that part of the medical scan. For instance, areas with high noise are more aggressive, and low noise areas have less aggression.

3.1.1. NLM Denoising

Non-Local Means (NLM) is a method that reduces noise and loss of significant picture information in lung cancer images. Pixel used similarity to compare areas and maintain similar features.

The method selects areas around the Region of Interest (ROI) using a window size of 21 x 21 pixels and a patch size of 7 x 7 pixels. The adaptive thresholding with a threshold value of 0.1 balances noise reduction with finer features.

The weight function used in image processing is based on the basic equation. The NLM noise reduction method aims to eliminate noise while minimizing the loss of fundamental information. Additionally, the given weight utilized during image processing increases with the degree of similarity. The NLM method's fundamental equation is represented as:

$$NLM|I(m| = \sum_{n\in N_m} \omega(N_m, N_n) I(n) \left(\omega(N_m, N_n) = \frac{1}{Z(m)} e^{-\frac{d}{h^2}} \right) \quad (1)$$

Where $I(n)$ is the intensity of the noise portion of the nth pixel, I(m) is the intensity at the pixel m in the image, N_mIs the area around them^{th} pixel, $\omega(N_m, N_n)$ is a function based on the weighted similarity (sum of the difference among the desired pixel and its neighbouring pixels), $Z(m)$ is the normalization constant, and d is the Euclidean distance.

3.1.2. Wavelet Denoising

Wavelet denoising is a technique used to train accurate prediction models for lung cancer detection. It involves three steps: decomposition, thresholding, and rebuilding. This method aims to eliminate high-frequency noise while preserving the lung cancer characteristics' general form and texture. It is a popular technique in time series denoising. The wavelet denoising approach involves three steps:

(1) Decomposition: Identify the wavelet basis function and the N decomposition layers.

(2) Threshold processing: Choose a threshold function, then calculate each layer's components.

(3) Reconstruction: By using the modified coefficients, reassemble the data.

The soft threshold and hard threshold parameters of the threshold function are defined in Equation (2) and Equation (3), respectively.

Soft threshold,

$$y_{new} = \begin{cases} sgn(y).(|y| - T), |y| \geq T \\ 0, |y| < T \end{cases} \quad (2)$$

Hard threshold,

$$y_{new} = \begin{cases} y, |y| \geq T \\ 0, |y| < T \end{cases} \quad (3)$$

Where y is the wavelet coefficient, T denotes the threshold, $|y|$ is the wavelet coefficient, and sgn(y) is the sign of y (positive or negative). The data will cause extra oscillation, and the hard threshold function will maintain the signal's peak characteristics. The wavelet coefficients do, however, maintain a higher level of overall continuity when using the soft threshold function, and the original signal's smoothness is also preserved. Consequently, the wavelet denoising approach uses a soft threshold function.

3.2. Image Augmentation using a GAN Model

To further enhance the dataset and improve model generalization, we employ DCGANs (Deep Convolutional Generative Adversarial Networks) for data augmentation. DCGANs produce synthetic pictures that are closely similar to real lung cancer images, diversifying the dataset and improving the categorization model's reliability. Deep Convolutional GAN for generating realistic medical images, especially for lung cancer detection. The discriminator distinguishes between original and produced images. The Adam optimizer was used for training, and IS and FID validated the model's performance. Domain specialists incorporated the produced photos into the dataset for further training. This includes the training parameters and how the DCGAN's performance was validated using metrics like Inception Score (IS) and Frechet Inception Distance (FID). The ability of DCGANs to recognize and comprehend patterns in the training data allows them to produce new data with comparable characteristics. A DCGAN, qualified on the collection of images, produces new pictures that seem truthful to a human observer. Generator and discriminator networks are both present in the DCGAN. The discriminator is given the capacity to discriminate between real samples and synthetic samples. Their purpose of min-max is represented by Equation (4) and uses the value function:

$$V(G, D): \min_G \max_D V(D, G) = E_{w\sim P_d(w)}[\log D(w)] + E_{y\sim P_y(y)}[\log(1 - D(G(y))] \quad (4)$$

Where y is the generated data samples produced by the generator G, w is the unaffected data model taken after$P_d(w)$, G and D are the generator and discriminator, $D(G(y))$ is the discriminator output for fake data generated by the G, and y is

the random (noise) input taken from $P_y(y)$. The discriminator Loss function (L_D) is a typical crossentropy loss function, similar to the double classifier given in Equation (5):

$$L_D = -(f \log(p) + (1-f)\log(1-p)) \quad (5)$$

Where L_D is the loss of the discriminator, f is a true table, p is the predicted probability that the input is real, $(1-f)\log(1-p)$ and is the loss when the true label is 0 (fake data), and the model predicts the probability p. The results of the loss function were very heterogeneous, dependent on the sorts of contribution examples employed. A number p displays the likelihood of properly forecasting the precise and big models, even if f denotes the initial digit. The loss generator (L_G) seeks to produce as many random variable quantities as conceivable to maximize the loss function of the discriminator (L_D). The ultimate purpose of the producer is articulated as $f \log\big(D(y)\big)$. The failure of the originator, which is shown in Equation 6:

$$(L_D) = = -\{(f \log\big(D(w)\big) + (1-f)\log(1 - Dis\big(G(y)\big))\} \quad (6)$$

Where $D(w)$ is the chance of the discriminator assigning to the real picture w, D ($G(y)$) is the possibility that the discriminator allocates to the produced (Fake) image from the originator$G(y)$, and $G(y)$ is the generated image from the generator based on input y. While training, only one model's parameters are changed, not those of the second. The generator functions most effectively when the discriminator becomes perplexed and is unable to distinguish between true samples and fake ones. After the drill, the discriminator is changed so that it functions best aimed at the current generator.

For training purposes, we used parameter values such as batch size, learning rate, beta1, epochs, image size, and the model's performance, which was validated using IS and FID. An IS is a higher Inception Score, which generally indicates better image quality and diversity.

A FID is a lower FID score, generally indicating that the generated images are more similar to the real images and thus more realistic. The ability of DCGAN to reproduce and create synthetic images allows it to compare the visual similarity to a real image. A sample of a synthetic image generated using DCGAN is shown in Figure 2. The quality evaluation of the DCGAN is summarized in Table 1.

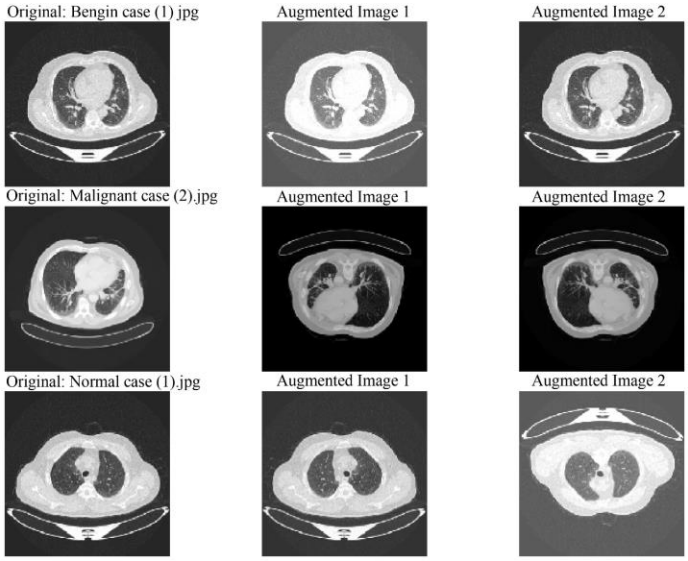

Fig. 2 Sample of a synthetic image generated using DCGAN

Table 1. Quality evaluation of DCGAN-generated CT images

Metric	Real CT Images	DCGAN Generated Images
Inception Score	2.85	2.71
Frechnet Inception Distance	-	32.5

3.3. ROI Extraction using ACE-ACM

The lung tumor regions, the Adaptive Correlation Enhanced Active Contour Model (ACE-ACM), are used to identify and segment lung tumor regions from medical images. This technique ensures that subsequent texture analysis focuses on relevant regions, improving classification accuracy in lung cancer diagnosis. By incorporating an adaptive local correlation map, ACE–ACM enhances the representation of tumor regions and suppresses background structures. The correlation-based term in the energy function

guides the contour toward true tumor boundaries, even in the presence of high noise, low contrast, and irregular nodule shapes. The ACE-ACM's contour-based methodology distinguishes and separates the tumor area from the surrounding area, making it suitable for medical imaging applications like object recognition and shape analysis. The study aims to isolate the ROI region from the rest, enhancing the accuracy of further texture analysis. The steps involved in the ACE-ACM are given below,

Step 1: Compute the weight function

The weight function of the pre-processed image is calculated using the adaptive weight function. The mathematical expression of the weight function is given in Equation (7) as,

$$E_{Contour} = \int (\alpha * w(s) * |\nabla|s|^2 - \beta * |\nabla^2|(s)|\, ds \quad (7)$$

Where $w(s)$ denotes the weight function, which is represented by,

$$w(s) = w_{base} + w_{gradient} * |\nabla|(s)| \quad (8)$$

Where α is a scaling factor, $\nabla|s|^2$ is the gradient of the squared intensity, β is the scaling factor for the Laplacian term, $|\nabla|s|^2|$ is Laplacian, smooths the contour,w_{base} represents the base weight of the pre-processed image, and $w_{gradient}$ denotes the weight factor that increases the gradient magnitude $|\nabla|(s)|$.

Step 2: Compute the cross-correlation-based entropy

After finding the weight function $E_{Contour}$, the crosscorrelation-based entropy ($H_{cress} - correlation$) is calculated using Equation (9) below,

$$H_{cress} - correlation = -\int (T(s) * \log(I_r(s))ds \quad (9)$$

Where $T(s)$ represents the template function that represents the expected appearance, $I_r(s)$ and denotes the image region around contour points.

Step 3:Modified energy function computation

The energy function $E_{total}$is calculated based on the contour value and the cross-correlation-based entropy value. Which is defined in Equation (10) as,

$$E_{total} = E_{Contour} + \gamma * H_{cress} - correlation \quad (10)$$

$$E_{total} = \int (\alpha * w(s) * |\nabla|s|^2 - \beta * |\nabla^2|(s)|\, ds + \gamma * (-\int (T(s) * \log(I_r(s))ds) \quad (11)$$

3.4. Feature Extraction

From the segmented pictures, useful characteristics can be extracted by an advanced feature extraction method. Instead of relying solely on traditional approaches, we integrate deep learning-based feature extraction models, such as pre-trained models like VGGNet and ResNet. These models automatically learn and extract high-level features from lung cancer images, capturing intricate patterns and improving classification accuracy.

3.4.1. VGG 16

The ImageNet dataset was utilized to pre-train the VGG16 model, which is used to extract constraint characteristics. The VGG16 construction comprises three fully connected layers after the primary five blocks of convolutional layers. To maintain identical spatial dimensions as the layer preceding it, respectively, start the map in a convolutional coating using a 33 kernel through a step of 1 and a padding of 1. With the help of the imported convolutional layer's parameters, the bottleneck characteristics are retrieved. Each difficulty is shadowed by a ReLU activation, a three-dimensional lowering by the max pooling technique. Max pooling layers employ 22 kernels with a pace of 2 and no padding to make sure every spatial measurement of the beginning map of the preceding layer is divided in half. After two linked coatings with 4,096 ReLU beginning units, the last 1,000 fully associated softmax coatings are rummage-sale. The VGG16 model has some downsides, including a high assessment cost and high memory and storage needs. VGG16 is then made up of 138 million or more parameters. The fully connected layers include 123 million occurrences of these traits.

3.4.2. ResNet

ResNet performs well in a diversity of requests, including speech acknowledgment, natural language dispensation, picture classification, image production, visual identification, and user prediction. Following two weight layers, the input value x's residual mapping is denoted by $H(x)$, and the fundamental mapping is denoted by $F(x)$, respectively. The residual unit converts the issue from matching the connection between $H(x)\ and\ x$ to fitting the connection between $F(x)\ and\ x$ by employing a function of identity as a shortcut link. Two different benefits of the residual network over the standard CNN are discussed below.

Easier to be Optimized

ReLU is the activation function placed before the output layer of the residual unit, which frequently acts as an intrinsic value of 0 or an identity function. For learning, we combined many leftover units. If one assumes that the identity functions that activate the ReLU are,

$$x_{l+1} = x_l + F(x_l, \{W_l\}) \quad (12)$$

Where W_l stands for the weights and x_l stands for the l^{th} resnet unit's input. A direct forward propagated output (x_{l+1}) and the residual mapping of the l^{th} resnet unit that has to be learnt is represented by $F(x_l, \{W_l\})$. Following that definition, the residual network's forward propagation mechanism is,

$$x_L = x_l + \sum_{i=l}^{L-1} F(x_l, \{W_l\}) \quad (13)$$

Where x_L is the total output of the connected residual units of length L. On the other hand, a typical CNN's forward propagation procedure may be characterized as,

$$x_L = x_l \prod_{i=l}^{L-1} W_i \quad (14)$$

In the formula, where Wi denotes the weights, x_l and x_L stand for the input and output of the lth $L1$ convolutional layer, respectively. Equation (13) and Equation (14) may be compared to show that the residual network requires less computing power and is optimized more easily than the conventional CNN.

A more effective approach to the gradient issue

According to Equation (13), the backpropagation procedure may be used to represent the gradient of the residual network as

$$\frac{\partial E}{\partial x_l} = \frac{\partial E}{\partial x_L}\left(1 + \frac{\partial}{\partial x_L}\sum_{i=l}^{L-1} F(x_i, \{W_l\})\right) \quad (15)$$

Where E stands for the model's loss function. The gradient of a standard CNN may be determined by,

$$\frac{\partial E}{\partial x_l} = \frac{\partial E}{\partial x_L}\prod_{i=l}^{L-1} W_i \quad (16)$$

The traditional CNN is prone to gradient disappearance and explosion issues as the network gets deeper, while the ResNet may successfully address these issues, according to the comparison between Equation (15), and (16).

3.5. Feature Selection using ScLnO

To optimize the feature space and reduce dimensionality, we utilize an advanced feature selection algorithm called the ScLnO algorithm. The proposed ScLnO algorithm is the combination of the SLO and SSA, respectively. These techniques intelligently identify the most relevant and discriminative features, safeguarding the classification of typical attentions on the most useful aspects of lung cancer images. Various kinds of sparrows are often social birds.

The producer and scrounger are two separate species of house sparrows that are kept as pets. While the scroungers rely on the producers to provide them with food, the producers actively seek sources of food. In the meantime, the predatory birds in the flock employ the partners with high intakes as competition for their food sources to increase their predation level. The behavior of the sea Lion is hybridized with the sparrow to improve the strategies of the sparrow.

Step 1: Initialization

To find food in the simulation experiment, we utilize computer-generated sparrows. The following matrix is used to show where sparrows are located:

$$X = \begin{bmatrix} X_1 \\ \vdots \\ X_i \\ \vdots \\ X_N \end{bmatrix}_{N\times m} = \begin{bmatrix} x_{1,1} & \cdots & x_{1,d} & \cdots & x_{1,m} \\ \vdots & \ddots & \vdots & \ddots & \vdots \\ x_{i,1} & \cdots & x_{i,d} & \cdots & x_{i,m} \\ \vdots & \ddots & \vdots & \ddots & \vdots \\ x_{N,1} & \cdots & x_{N,d} & \cdots & x_{N,M} \end{bmatrix}_{N\times m} \quad (17)$$

where n is the total number of sparrows, and d represents the dimension of the parameters that have to be optimized.

Step 2: Fitness computation

The fitness of the optimization is computed by using the accuracy value. The mathematical expression for the fitness is given in Equation (18),

$$Fitness = 1/Accuracy \quad (18)$$

Consequently, the following vector may be used to represent the fitness value for all sparrows:

$$F_X = \begin{bmatrix} f(x_{1,1} & \cdots & x_{1,d} & \cdots & x_{1,m}) \\ \vdots & \ddots & \vdots & \ddots & \vdots \\ f(x_{i,1} & \cdots & x_{i,d} & \cdots & x_{i,m}) \\ \vdots & \ddots & \vdots & \ddots & \vdots \\ f(x_{N,1} & \cdots & x_{N,d} & \cdots & x_{N,M}) \end{bmatrix}_{N\times m} \quad (19)$$

This shows the individual's level of fitness as measured by the length of each row in FX, while n here stands for the number of sparrows. When searching for food in the SSA, producers with higher fitness ratings are given preference. Furthermore, the producers are assumed to be the first 10% of the fitness solutions since they are in charge of directing the scroungers and seeking food. The other 40% of the fitness solution is classified as scroungers since they follow the producers' lead and create the majority of the population's food. In contrast to scroungers, producers have a greater range of options regarding where to seek food.

Step 3: Sealion-based Detection and tracking of prey by scroungers. Using a uniform random distribution in the search space, SLO first creates N (the population's size) D-dimensional solutions as shown below. Then, the producers locate the prey and attract other members to form the subgroup before organizing the net in accordance with the encircling process. The best current option-or the solution that comes

closest to becoming the best solution-is regarded as the prey. Equation (20) presents these behaviours.

$$X_{i,j}^{new} = X_{i,j}^{min} + E * P * (X_{i,j}^{max} - X_{i,j}^{min}) \quad (20)$$

Where $i = 1,2,\dots,N$ and $j = 1,2,\dots,D$. $X_{i,j}^{min}$ represents the minimum value of the i^{th} solution with j^{th} dimension, similarly, $X_{i,j}^{max}$ is the maximum value of the i^{th} solution with j^{th} dimension, E is the encircling factor that controls the step size of the movement. Then the parameter P represents the promising area.

Step 4: Producer-Scrounger interaction based on vocalization

A Producer will summon other Scroungers in its group to come together and construct a net to catch the prey when it spots a gathering of its prey. The Producer is regarded as the group's leader and will direct the Scrounger group's actions and determine its behavior. The producers' instructions serve as the basis for the Scroungers' positional adjustments. The vocalization behavior of the SLO is hybrid with the interaction phase of the Producer-Scrounger. Vocalization plays a vital role in the interaction between producers and scroungers, facilitating communication and coordination of foraging activities. These behaviors are represented mathematically in Equation (21),

$$S_{ij}^{new} = S_{ij} * \left|\frac{V_1(1+V_2)}{V_2}\right| + G * \left(X_{ij} - P_{ij}\right) \quad (21)$$

Where G is the guidance factor, S_{ij} which signifies the location of the scrounger, X_{ij} which denotes the situation of the producers. The values of V_1 and V_2 are given in Equation (22) and Equation (23), respectively.

$$V_1 = \sin\theta \quad (22)$$

$$V_2 = \sin\phi \quad (23)$$

Whereθ is the angle of voice reflection, ϕ is the angle of voice refraction. In our research, r is a randomly generated number between [0, 1], $\theta = 2r$, and $\phi = 2(1-r)$.

Step 5: Attacking phase (Circling, updating position founded on the disordered map).

The producer hunts the bait ball of prey by starting at the boundaries and pursuing it. Constructed on a tent-like, disordered map, the position of the circling is updated. The fundamental solution, the current optimal solution, is used to create the tent chaotic sequence. The ideal solution in the series is then utilized to update the position of the food supply, forcing it to depart from the local optimal. In Equation (24), the mathematical expression is represented as,

$$X_{ij} = X_{best} + \cos(2\pi m) * \left|X_{gbest} - X_{best}\right| \quad (24)$$

Where m is the tent chaotic map, X_{best} is the best solution. and $X_{g\ best}$ is the global best solution.

Step 6: Position update of the Scrounger

Certain scroungers pay more attention to the producers. They leave their present place as soon as they learn that the producer has discovered excellent food and begin fighting for it. They rapidly obtain the food created if they are successful; if not, the laws are still followed. The method for changing the location of the scrounger is provided in Equation (25) below:

$$X_{ij}^{t+1} = \begin{cases} Q.\exp\left(\frac{x_{worst}^{t} - X_{ij}^{t}}{i^2}\right) if\, i > n/2 \\ X_P^{t+1} + \left|X_{i,j}^{t} - X_P^{t+1}\right|.A^{+}.L,\ Otherwise \end{cases} \quad (25)$$

Where XP denotes the producer's ideal position. x_{worst}^{t} designates the world's worst location at the moment. Each member in the 1,d matrix A is given a random number between -1 and 1, and $A^{+} = A^{T}(AA^{T})^{-1}$. The i^{th} scrounger with the lowest fitness grade has a higher chance of going hungry when $i > n/2$.

Step 7: Except for the so far developed best solution.

Step 8: Return the best resolution

Step 9: Terminate condition

Algorithm 1:Pseudocode of ScLnO algorithm

Step 1: Initialization
X[N][m] = Initialize Sparrows PositionMatrix() // Equation (17)
Step 2: Fitness Computation
F_X[N][m] = CalculateFitness Matrix(X) // Equation (18), Equation (19)
Step 3: Detection & Tracking of Prey by Scroungers
Initialize Solutions(X) // Equation (20)
Step 4: Producer-Scrounger Interaction based on Vocalization
Update Scrounger Positions(X) // Equation (21)
Step 5: Attacking Phase (Updating Position based on Tent Chaotic Map)
Update Producer Positions(X) // Equation (24)
Step 6: Position Update of the Scrounger
Update Scrounger Positions Based on Conditions(X) // Equation (25)
Step 7: Save the Best Solution So Far
Save Best Solution(X)
Step 8: Return the Best Solution
Return Best Solution(X)
Step 9: Terminate Condition
if Termination ConditionMet() then
Terminate Simulation()

After performing the feature assortment task, the selected optimal features were used for the DenseEnsembleNet classifier for categorizing disease images. For this classification purpose, the hyperparameters of the DenseNet model are fine-tuned using the ScLnO algorithm.

3.6. Lung Cancer Classification using DenseEnsembleNet

This DenseEnsembleNet is the combination of the optimized DenseNet and CNN. DenseNet models facilitate feature reuse and gradient flow, enabling effective learning and representation of complex patterns in lung cancer images. We fine-tune the DenseNet model using advanced optimization algorithms, which optimize the network's weights and improve the overall classification performance. The architecture of the DenseEnsembleNet is shown in Figure 3.

Features extracted from images from ScLnO were passed to DenseEnsembleNet(OptimizedDenseNet + CNN). Once the image enters the novelty net (DenseEnsembleNet), the novelty net consists of DenseNet and CNN. DenseNet will receive the feature extraction image, and the CNN also receives the same image. DenseNet was started to fine-tune the image properties and provide the output feature extraction image, and at the same time, Convolutional Neural Networks were used to find the pattern, and the image was extracted with spatial resolution features, and provide an output of the feature extracted image. Both the output image was passed through the concatenate layer. The combination helps to ensure that the detection and classification of lung types perform extraordinarily. The hyperparameter configuration and its justification are given in Table 2.

Table 2. Hyper parameter configuration and justification

Hyper Parameter	Value Used	Justification
Learning Rate	0.001	Stable Convergence for dense architecture
Batch size	128	Efficient Training
Optimizer	Adam Optimizer	For smooth Convergence
Number of dense blocks	4	Balanced Depth
Growth rate	32	Strong feature reuse
Dropout	0.2	Prevents Overfiting

3.6.1. Optimized DenseNet

The DenseNet consists of convolutional layers, dense layers (completely linked layers), maxpool layers, and convolutional layers. The architecture of the perfect is activated with ReLU throughout, and the top layer is activated with SoftMax.

The convolutional layers restore the properties of the picture while the maxpool layers lower the dimensionality of the input.

The fully associated layers come after the initial flattened coating in the stack. One input array is sent to the compression layer, which performs as an ANN. The hyperparameters of the DenseNet model, like Number of layers, Batch size, and Learning rate, are fine-tuned using the ScLnO algorithm.

Figure 4 provides illustrative examples showcasing the sequential analysis of two distinct sample images, each representing a specific scenario in lung cancer detection.

The first image in the sequence corresponds to a healthy lung, while the second image portrays a lung affected by cancerous growth. Each of these images undergoes a step-by-step process to elucidate the identification process comprehensively.

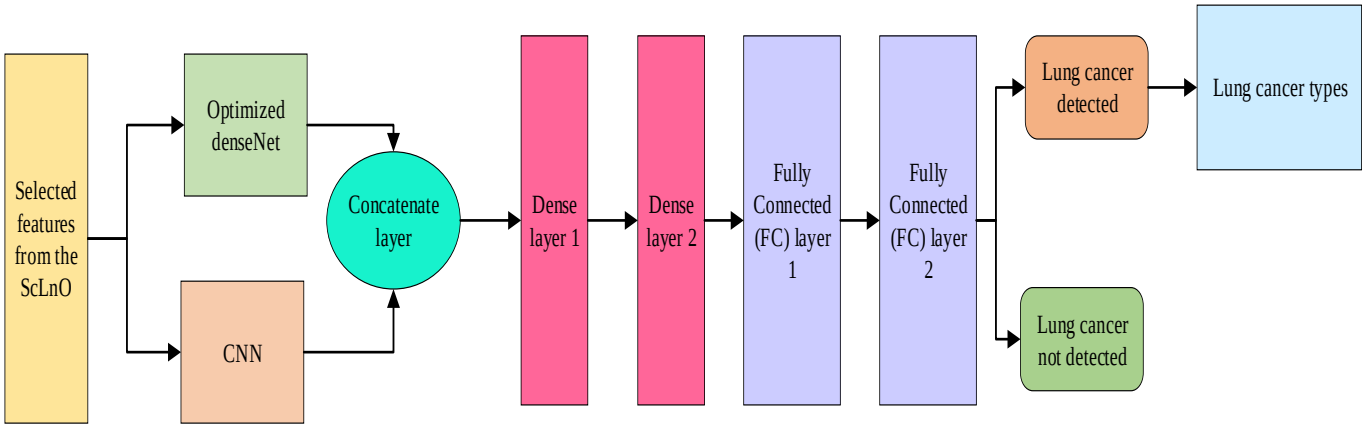

Fig. 3 Layered architecture of the DenseEnsembleNet

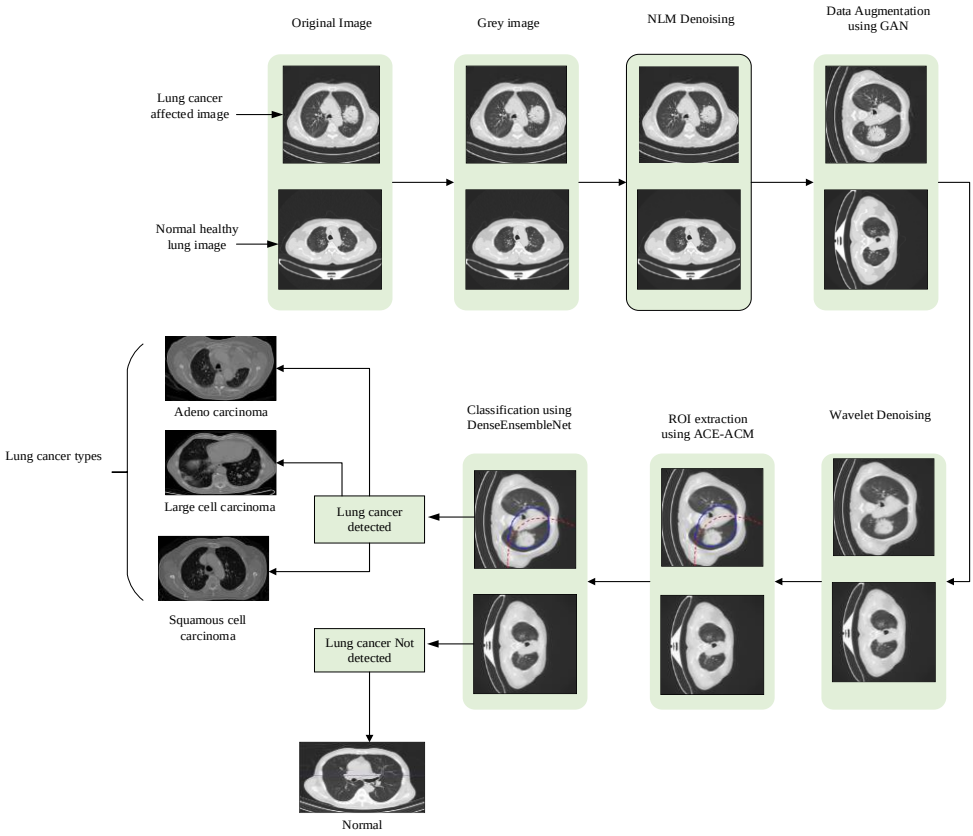

Fig. 4 Input image at each stage

4. Result and Discussion

4.1. Performance Metrics

The calculation formulas for performance metrics are provided below.

Sensitivity

Simply divide the entire positives by the number of true optimistic predictions to get the warmth number.

$$Sensitivity = \frac{TP}{TP+FN} \quad (40)$$

Specificity

By precisely separating the numbering of anticipated negative results by the entire amount of rejections, one may determine the specificity of a forecast.

$$\text{Specificity} = \frac{\text{TN}}{\text{TN+FP}} \quad (41)$$

Accuracy

The correctness is determined by dividing the amount of successfully sorted data by the total amount of data in the stream. The definition of the degree of precision is,

$$Accuracy = \frac{TP+TN}{TP+FP+FN+TN} \quad (42)$$

Precision

It is a whole quantity of honest values that are suitably taken into deliberation during the organization stage, utilizing all samples used in the classification technique.

$$Precision = \frac{TP}{TP+FP} \quad (43)$$

Recall

The recall rate is a measure of how many real examples were used to classify the training data when every sample from the same group was used.

$$Recall = \frac{TP}{TP+FN} \quad (44)$$

F- Measure

Parametric methods for the F-measure, a special instance of F_β with β = 1, aiming to improve the sensitivity and efficiency of these methods when the assumptions are correct.

$$F_{Measure} = \frac{2\,Precision \times Recall}{Precision+Recall} \quad (45)$$

Negative Prediction Value (NPV)

NPV designates the efficiency of an analytic test or similar measurable metric.

$$NPV = \frac{TN}{TN+FN} \quad (46)$$

Matthew's correlation coefficient (MCC)

The two-by-two dual factor correlation measurement, occasionally mentioned as MCC, is shown in the equation below,

$$MCC = \frac{(TP \times TN - FP \times FN)}{\sqrt{(TP+FN)(TN+FP)(TN+FN)(TP+FP)}} \quad (47)$$

False Positive Ratio (FPR)

The amount of negative events divided by the total number of undesirable occurrences is inadvertently converted into positive results.

$$FPR = \frac{FP}{FP+TN} \quad (48)$$

False Negative Ratio (FNR)

FNR, often recognized as "miss rate," indicates the possibility that an actual positive will not be detected by the test.

$$FNR = \frac{FN}{FN+TP} \quad (49)$$

Additionally, the component-wise performance analysis has been done to ensure the novelty of the research work and is submitted in Table 3.

Table 3. Component-wise performance analysis of the proposed method

Model Version	Accuracy
Full Model	98.5
Without DCGAN	92.5
Without ACE-ACM	89.4
CNN	85.6

This next section compares the suggested method's outcomes to those from the currently used approaches. In this work, there are two types of datasets used. Dataset 1 is used to predict whether lung cancer is present or not, and dataset 2 is used to predict the type of lung cancer. The detailed description of the two datasets is given below. Dataset 1The IQ-OTH/NCCD lung cancer dataset(2023) [26] is taken as the input image, and the PYTHON platform is employed for implementation.

The IQ-OTH/NCCD lung cancer dataset, which includes CT scans from both lung cancer patients and healthy participants, was gathered from specialized hospitals over the course of three months in 2019. The dataset consists of 1190 CT scan shares from 110 examples that have been secret as kind, mean, or standard deviation by medical professionals. Siemens SOMATOM scanners were used to acquire the scans, and a precise CT procedure was followed. Implementation of privacy safeguards was approved by the institutional review board. Each case includes many chest slices, and the dataset represents the variety of occupations and demographics in Iraq, offering a thorough resource for lung cancer research. The whole amount of data is divided into two groups, termed training and testing.

The remaining 30% of the data is utilised for testing, with the remaining 70% being used for training. The performance metrics are used for the evaluation of Dataset 2. The second dataset is the ChestCT-Scan images Dataset (2023) [27]. Data are used in three different ways: 70% for training, 20% for testing, and 10% for other purposes. The dataset for the chest cancer detection project consists of medical images in JPG or PNG format, rather than the DICOM format, to align with the necessities of the machine learning model. It encompasses images related to three distinct chest cancer types, namely large cell carcinoma, Adenocarcinoma, and Squamous cell carcinoma. Additionally, there is a folder containing images representing normal chest cells. The dataset has been meticulously collected and cleaned from various sources, ensuring its suitability for keeping fit and evaluating the CNN-based design for chest cancer arrangement and diagnosis. Overall comparison of the proposed lung cancer detection model (ScLnO+ DenseEnsembleNet) is associated with the existing methods like SVM, SLO, SSA DenseEnsembleNet, and the proposed classifier (Pro-classifier). The comparison is shown in Tables 4 and 5.

Table 4. Overall assessment of the proposed lung cancer detection model (Dataset 1)

Metrics	CNN	SVM	DenseEnsembleNet	SLO	SSA	Proposed
Accuracy	0.979	0.856	0.978	0.945	0.923	0.987
Precision	0.969	0.848	0.978	0.918	0.884	0.974
Sensitivity	0.969	0.823	0.962	0.918	0.884	0.97
Specificity	0.979	0.826	0.982	0.959	0.942	0.989
F-Measure	0.969	0.823	0.978	0.918	0.884	0.987
MCC	0.954	0.812	0.968	0.877	0.827	0.981
NPV	0.984	0.809	0.989	0.959	0.942	0.993
FPR	0.015	0.062	0.010	0.040	0.057	0.006
FNR	0.030	0.092	0.021	0.081	0.115	0.012

Table 5. Overall assessment of the proposed lung cancer classification model (Dataset 2)

Performance metrics	CNN	SVM	DenseEnsembleNet	SLO	SSA	Proposed
Accuracy	0.977	0.850	0.985	0.955	0.913	0.988
Precision	0.966	0.775	0.978	0.933	0.869	0.985
Sensitivity	0.966	0.775	0.978	0.933	0.869	0.984
Specificity	0.983	0.887	0.989	0.966	0.934	0.989
F-Measure	0.966	0.775	0.978	0.933	0.869	0.984
MCC	0.9500	0.6636	0.9682	0.9000	0.804	0.985
NPV	0.983	0.887	0.984	0.966	0.934	0.985
FPR	0.016	0.112	0.010	0.033	0.06	0.003
FNR	0.033	0.224	0.021	0.066	0.130	0.006

4.2. Statistical Performance Analysis

Thorough statistical research was carried out to guarantee the robustness and dependability of the suggested lung cancer classification framework. In order to capture performance variability across various data splits, the model's performance was assessed using 5-fold cross-validation. The findings are shown in terms of mean and standard deviation(SD). It is discussed in Table 6.

Table 6. Statistical validation of results

Metric	Mean %	SD %	Confidence Interval %	Statistical Significance
Accuracy	98.5	±0.6	[97.4, 98.9]	P<0.01
Precision	97.5	±0.8	[95.9, 98.9]	P<0.01
Sensitivity	98.8	±0.5	[97.8, 98.7]	P<0.01
Specificity	98.2	±0.7	[96.8, 98.7]	P<0.01
F-Measure	98.0	±0.6	[96.8, 99.1]	P<0.05

5. Conclusion

Accurate lung cancer classification is crucial for effective management planning and positive patient outcomes due to its prevalence and life-threatening nature. The study introduces a groundbreaking methodology that integrates advanced technologies in deep learning, feature extraction, and image processing. Our approach utilizes advanced denoising techniques and GANs for dataset augmentation, enhancing image quality, and improving model generalization. The ACE-ACM and ScLnO hybrid optimization algorithms enhance ROI identification, feature extraction, and analysis processes by intelligently identifying key features. The classification stage utilizes the DenseEnsembleNet, a combination of Optimized DenseNet and CNN, resulting in exceptional accuracy. The innovative framework has the potential to revolutionize lung cancer diagnosis with a remarkable 98.7% - 98.8% accuracy rate, surpassing existing techniques. The integration of advanced technologies in lung cancer classification has led to a robust and promising solution, enhancing medical diagnostics and patient care. The suggested approach could help radiologists make decisions by aiding in the early identification of lung cancer from CT scans. The use of ensemble-based learning improves resilience by lowering model variance; nonetheless, applicability to previously unreported clinical data cannot be completely assured without external multi-centre validation. Despite the performance of the proposed framework, it is limited to the publicly available dataset.

References

[1] M. Braveen et al., "Retracted Article: ALBAE Feature Extraction-Based Lung Pneumonia and Cancer Classification," *Soft Computing*, vol. 28, no. S2, 2023. [CrossRef] [Google Scholar] [Publisher Link]

[2] Chiagoziem C. Ukwuoma et al., Automated Lung-Related Pneumonia and COVID-19 Detection based on Novel Feature Extraction Framework and Vision Transformer Approaches using Chest X-ray Images," *Bioengineering*, vol. 9, no. 11, pp. 1-27, 2022. [CrossRef] [Google Scholar] [Publisher Link]

[3] Birger Tielemans et al., "From Mouse to Man and Back: Closing the Correlation Gap between Imaging and Histopathology for Lung Diseases," *Diagnostics*, vol. 10, no. 9, pp. 1-25, 2020. [CrossRef] [Google Scholar] [Publisher Link]

[4] Konstantinos P. Exarchos et al., "Recent Advances of Artificial Intelligence Applications in Interstitial Lung Diseases," *Diagnostics*, vol. 13, no. 13, pp. 1-13, 2023. [CrossRef] [Google Scholar] [Publisher Link]

[5] Rajneesh Kumar Patel, and Manish Kashyap, "Automated Diagnosis of COVID Stages from Lung CT Images using Statistical Features in 2-Dimensional Flexible Analytic Wavelet Transform," *Biocybernetics and Biomedical Engineering*, vol. 42, no. 3, pp. 829-841, 2022. [CrossRef] [Google Scholar] [Publisher Link]

[6] Aya Hage Chehade et al., "Lung and Colon Cancer Classification using Medical Imaging: A Feature Engineering Approach," *Physical and Engineering Sciences in Medicine*, vol. 45, no. 3, pp. 729-746, 2022. [CrossRef] [Google Scholar] [Publisher Link]

[7] Abdulrazak Yahya Saleh et al., "Lung Cancer Medical Images Classification using Hybrid CNN-SVM," *International Journal of Advances in Intelligent Informatics*, vol. 7, no. 2, pp. 151-162, 2021. [CrossRef] [Google Scholar] [Publisher Link]

[8] Yahia Said et al., "Medical Images Segmentation for Lung Cancer Diagnosis based on Deep Learning Architectures," *Diagnostics*, vol. 13, no. 3, pp. 1-15, 2023. [CrossRef] [Google Scholar] [Publisher Link]

[9] RuoXi Qin et al., "Fine-Grained Lung Cancer Classification from PET and CT Images based on Multidimensional Attention Mechanism," *Complexity*, vol. 2020, no. 1, pp. 1-12, 2020. [CrossRef] [Google Scholar] [Publisher Link]

[10] Shixuan Zhao et al., "SCOAT-Net: A Novel Network for Segmenting COVID-19 Lung Opacification from CT Images," *Pattern Recognition*, vol. 119, pp. 1-12, 2021. [CrossRef] [Google Scholar] [Publisher Link]

[11] Conor Wall et al., "A Deep Ensemble Neural Network with Attention Mechanisms for Lung Abnormality Classification using Audio Inputs," *Sensors*, vol. 22, no. 15, pp. 1-25, 2022. [CrossRef] [Google Scholar] [Publisher Link]

[12] Jiaxing Sun et al., "Detection and Staging of Chronic Obstructive Pulmonary Disease using a Computed Tomography-based Weakly Supervised Deep Learning Approach," *European Radiology*, vol. 32, no. 8, pp. 5319-5329, 2022. [CrossRef] [Google Scholar] [Publisher Link]

[13] Ahmed Shaffie et al., "Computer-Assisted Image Processing System for Early Assessment of Lung Nodule Malignancy," *Cancers*, vol. 14, no. 5, pp. 1-22, 2022. [CrossRef] [Google Scholar] [Publisher Link]

[14] Scott J. Adams et al., "Clinical Impact and Generalizability of a Computer-Assisted Diagnostic Tool to Risk-Stratify Lung Nodules with CT," *Journal of the American College of Radiology*, vol. 20, no. 2, pp. 232-242, 2023. [CrossRef] [Google Scholar] [Publisher Link]

[15] Judith Juan et al., "Computer-Assisted Diagnosis for an Early Identification of Lung Cancer in Chest X Rays," *Scientific Reports*, vol. 13, no. 1, pp. 1-7, 2023. [CrossRef] [Google Scholar] [Publisher Link]

[16] Gopi Kasinathan, and Selvakumar Jayakumar, "Cloud-Based Lung Tumor Detection and Stage Classification using Deep Learning Techniques," *BioMed Research International*, vol. 2022, no. 1, pp. 1-17, 2022. [CrossRef] [Google Scholar] [Publisher Link]

[17] R. Sujitha, and V. Seenivasagam, "Retracted Article: Classification of Lung Cancer Stages with Machine Learning Over Big Data Healthcare Framework," *Journal of Ambient Intelligence and Humanized Computing*, vol. 12, no. 5, pp. 5639-5649, 2020. [CrossRef] [Google Scholar] [Publisher Link]

[18] A. Asuntha, and Andy Srinivasan, "Deep Learning for Lung Cancer Detection and Classification," *Multimedia Tools and Applications*, vol. 79, no. 11-12, pp. 7731-7762, 2020. [CrossRef] [Google Scholar] [Publisher Link]

[19] Dina M. Ibrahim, Nada M. Elshennawy, and Amany M. Sarhan, "Deep-Chest: Multi-Classification Deep Learning Model for Diagnosing COVID-19, Pneumonia, and Lung Cancer Chest Diseases," *Computers in Biology and Medicine*, vol. 132, pp. 1-14, 2021. [CrossRef] [Google Scholar] [Publisher Link]

[20] Vinod Kumar, and Brijesh Bakariya, "Classification of Malignant Lung Cancer using Deep Learning," *Journal of Medical Engineering & Technology*, vol. 45, no. 2, pp. 85-93, 2021. [CrossRef] [Google Scholar] [Publisher Link]

[21] Pankaj Nanglia et al., "A Hybrid Algorithm for Lung Cancer Classification using SVM and Neural Networks," *ICT Express*, vol. 7, no. 3, pp. 335-341, 2021. [CrossRef] [Google Scholar] [Publisher Link]

[22] Panagiotis Marentakis et al., "Lung Cancer Histology Classification from CT Images based on Radiomics and Deep Learning Models," *Medical & Biological Engineering & Computing*, vol. 59, no. 1, pp. 215-226, 2021. [CrossRef] [Google Scholar] [Publisher Link]

[23] Imran Shafi et al., "An Effective Method for Lung Cancer Diagnosis from CT Scan using Deep Learning-Based Support Vector Network," *Cancers*, vol. 14, no. 21, pp. 1-18, 2022. [CrossRef] [Google Scholar] [Publisher Link]

[24] Bhoj Raj Pandit et al., "Deep Learning Neural Network for Lung Cancer Classification: Enhanced Optimization Function," *Multimedia Tools and Applications*, vol. 82, no. 5, pp. 6605-6624, 2023. [CrossRef] [Google Scholar] [Publisher Link]

[25] Mustafa Bicakci et al., "Metabolic Imaging based Sub-Classification of Lung Cancer," *IEEE Access*, vol. 8, pp. 218470-218476, 2020. [CrossRef] [Google Scholar] [Publisher Link]

[26] Hamdalla F. Al-Yasriy, The IQ-OTH/NCCD Lung Cancer Dataset, Kaggle, 2021. [Online]. Available: https://www.kaggle.com/datasets/hamdallak/the-iqothnccd-lung-cancer-dataset

[27] MengzhangLI, Chest CT-Scan Images, Awesome-Medical-Dataset, GitHub, 2025. [Online]. Available: https://github.com/openmedlab/Awesome-Medical-Dataset/blob/main/resources/ChestCT-Scan_images.md